J. Fluid Mech. (1969), *vol.* 36, *part* 4, *pp.* 639–655
Printed in Great Britain

Mixing shocks in two-phase flow

By JAN H. WITTE
Hydronautics Incorporated, Laurel, Maryland, U.S.A.

(Received 22 October 1963 and in revised form 23 December 1968)

In gas–liquid flows a certain sudden change of the flow structure may occur, which can be described as a transition from 'jet flow' to 'froth flow' accompanied by energy dissipation and pressure build-up. Upstream of this phenomenon the gas is the continuous phase; downstream the liquid is the continuous phase. The phenomenon, which has been called 'mixing shock', shows some similarity and also some differences with the plane shock wave in gasdynamics. In the first part of this paper the mixing shock is treated as a one-dimensional macroscopic process. With the aid of the laws of conservation of mass, momentum and energy, expressions are obtained for the pressure and entropy change across the mixing process. In addition the stability of the mixing shock in a cylindrical flow channel is treated. Next, a theory that explains the gas entrainment mechanism in the mixing shock is proposed. As an experimental tool a water–air ejector with the water as a driving medium was used. The experiments confirm the macroscopic and the microscopic theory. In the last section of this paper theoretical and experimental evidence is combined to construct a model of the processes that play a role in the shock.

1. Introduction

In certain two-phase flow configurations a particular change of the flow structure may occur. This structure change may best be described as a sudden change of jet flow to froth flow accompanied by a static pressure increase and energy dissipation. The jet flow is characterized by a core of fast-moving liquid droplets surrounded by gas. In general a velocity difference or slip will exist between the gaseous and liquid phases. Froth flow consists of liquid in which the gas is dispersed in the form of bubbles. The diameters of these bubbles are small compared with the diameter of the flow channel. The slip between the bubbles and the surrounding liquid is very small.

The author of the present paper has named this phenomenon the mixing shock. Since the change of continuous phase is extremely rapid the term 'shock' is applied. The word 'mixing' is used because the gas phase is finely dispersed in the liquid when it passes through this flow discontinuity.

Von Pawell (1936) first observed the phenomenon through the transparent wall of a liquid–gas ejector and mentioned this in his thesis. Apart from its considerable technical interest for the isothermal compression of gases (Witte 1962,

1965, 1966), a close study of the mixing shock is valuable for obtaining an insight into the often mystifying behaviour of two-phase flows.

The mixing shock shows some similarity and also some differences with the plane shock wave in gasdynamics. The following characteristics are similar: (i) downstream of the mixing shock the pressure is higher and the velocities are lower than upstream; (ii) this effect is accompanied by dissipation of kinetic energy; (iii) when the mixture that is created in the shock is treated as being homogeneous with a special equation of state, it may be proved with a macroscopic theory that the flow downstream of the shock is always subsonic.

The most important differences are: (i) owing to the high specific heat of the liquid phase, the temperature changes across such a shock are extremely small; (ii) before the mixing shock an appreciable velocity difference or slip between the liquid and the gaseous part of the flow will generally exist. Thus we cannot speak of a homogeneous mixture, nor can we speak of supersonic mixture flow before the shock. Upstream of the shock the gas velocity may be higher than the liquid velocity; (iii) the mixing shock is much thicker than a shock wave in gasdynamics.

Campbell & Pitscher (1958) investigated the propagation of plane shock waves in a homogeneous gas–liquid mixture. Applying the laws of conservation of mass, momentum and energy, they derived shock-wave relations. In this paper we will use the same approach as Campbell & Pitscher in treating the case of the mixing shock. However, it must be kept in mind that, compared with plane shock waves in two-phase mixtures, we have one parameter more, viz. the velocity difference between the gas and liquid phase before entering the mixing shock. Other subjects that will be covered are the stability of a mixing shock situated in a cylindrical flow channel and the microscopic gas entrainment mechanism.

Experimental evidence was collected with a liquid–gas ejector, see figure 1. The gas flows through feed pipe d to the suction chamber b and is entrained in the mixing shock e. The mixing shock can be placed anywhere in the flow channel by applying back pressure. In order to obtain easy-to-measure pressures and to diminish the influence of gravity on the flow phenomena in the horizontal mixing tube, high jet flow speeds were used, of the order of 30–70 m/sec. The static pressure in the jet flow and the suction chamber was generally below ambient; after the shock the static pressure in the mixture could reach a level of up to 12 atmospheres.

2. The isothermal model

Before writing down the equations which govern the behaviour of the shock, we have to elaborate on the assumptions on which the theory will be based.

First, the flow of the gas and the liquid upstream and downstream of the mixing shock is assumed to be continuous. This property becomes exact when the number of droplets or gas bubbles passing a reference plane perpendicular to the flow direction per unit time is infinitely large and their dimensions infinitely small. In practice, this number is so large that the entrained gas mass flow is not subject to measurable fluctuations.

Furthermore, the flow is assumed to be one-dimensional and the influence of gravity is neglected.

It is also assumed that the temperature in a cross-section through the flow channel is constant. This assumption may be made plausible by pointing out that the contact surface between the gas and the liquid part of the flow is very large.

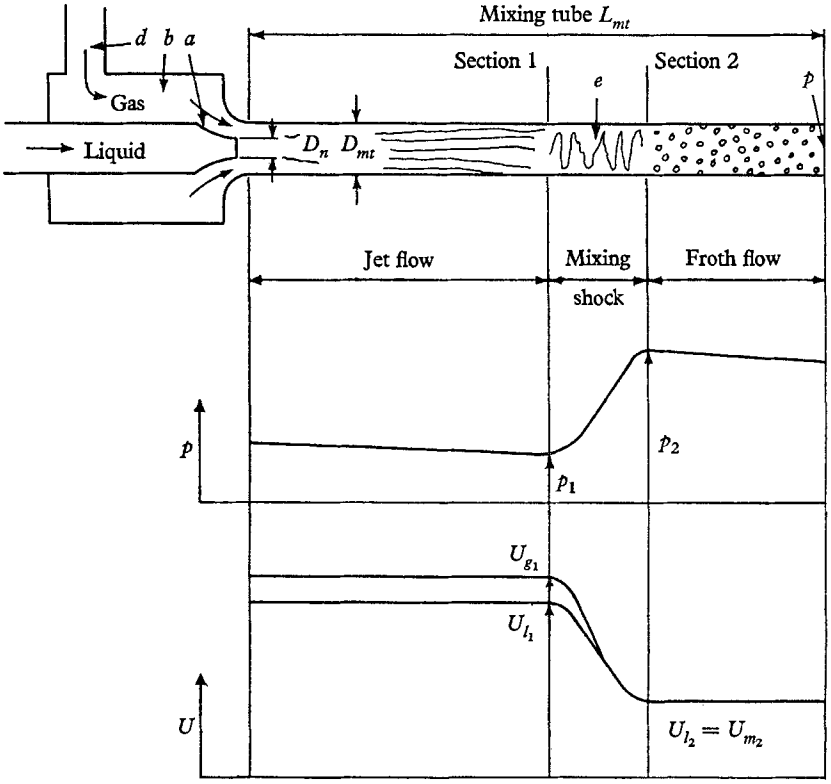

FIGURE 1. Schematic view of the experimental set up.

The influence of the vapour pressure and the viscosity of the gas and the liquid will be neglected. Wall friction will also be neglected. However, we point out that wall friction is important in stability considerations and will be introduced in § 4. In this section the temperature differences in the direction of the flow are assumed to be zero. In § 3 these differences are calculated for our experiments to be of the order of 0·1 degK.

We shall neglect the excess pressure caused by the surface tension in the bubbles in the mixture after the shock. The withdrawal of surface tension energy from the total energy of the flow will also be neglected. However, in § 6, it will be shown that the relatively small contributions of the surface tension effects in the energy balance can be used for calculating the gas-volume rate entrained by the mixing shock.

In the following considerations it will be assumed that the liquid is incompressible and that the gas follows the ideal gas law. The mass flow rate of the gas

is very small compared with the liquid mass flow rate and will be neglected. Slip between the gas bubbles and the liquid in the mixture after the shock will be neglected.

Two reference planes are chosen, one upstream and one downstream of the shock. To the downstream conditions we will attach subscript 1, to the upstream conditions subscript 2. Subscripts l, g and m will be used for denoting properties of the liquid, gas and mixture respectively. Subscripts n and mt refer to nozzle and mixing tube. Absolute pressure, speed and density are given by p, u and ρ. Cross-sectional area, mass flow rate and volume flow rate are denoted by A, M and Q; see also figure 1.

Using the above given assumptions we can write down the following relationships:

Continuity equation
$$M_{l_1} = M_{l_2}. \tag{2.1}$$

Momentum equation
$$p_1 A_{mt} + M_{l_1} u_{l_1} = p_2 A_{mt} + M_{l_2} u_{l_2}. \tag{2.2}$$

Equation of state of the mixture
$$\rho_{m_2}/\rho_l = (p_2/p_1)/\{(p_2/p_1) + (Q_{g_1}/Q_l)\}. \tag{2.3}$$

Energy equation
$$T_{l_1} = T_{l_2}. \tag{2.4}$$

It is seen that the presence of the gas phase only influences (2.3). In order to simplify the following calculations we define the superficial liquid velocity in the mixing tube: $u^* = M_l/\rho_l A_{mt}$; and the following dimensionless quantities:

$\epsilon = p_2/p_1$, compression ratio across the mixing shock;

$a = \rho_l u^{*2}/p_1$, Euler number before the shock;

$\theta = Q_{g_1}/Q_l$, volume flow rate before the shock;

$S = u_{g_1}/u_{l_1}$, slip factor before the shock;

$\alpha_2 = \rho_{m_2}/\rho_l$, mixture/liquid density ratio;

$\phi = A_n/A_{mt}$, nozzle/mixing tube area ratio;

$f = (A_{mt} - A_n)/A_n$, a useful area ratio.

Combining (2.1) and (2.2) and introducing ϵ, a, ϕ, θ and α_2 in (2.2) and (2.3) yield
$$\epsilon = 1 + a\left(\frac{1}{\phi} - \frac{1}{\alpha_2}\right), \tag{2.5}$$

$$\alpha_2 = \epsilon/(\epsilon + \theta). \tag{2.6}$$

Combining (2.5) and (2.6) we derive for the gas–liquid volume flow ratio upstream of the shock
$$\theta = (1/a)\{-\epsilon^2 + \epsilon(1 + af)\}, \tag{2.7}$$

which is related to the slip factor according to
$$S = \theta/f. \tag{2.8}$$

In a (θ, ϵ)-diagram (2.7) represents a bundle of parabolas with the Euler number a as parameter and a given value of f; see figure 2. The parabolas have two points in common,

$$\epsilon = 0, \quad \theta = 0 \quad \text{and} \quad \epsilon = 1, \quad \theta = f. \tag{2.9}$$

The top of each parabola is given by the co-ordinates

$$\epsilon_{\text{top}} = \tfrac{1}{2}(1+af), \quad \theta_{\text{top}} = (1+af)^2/4a. \tag{2.10}$$

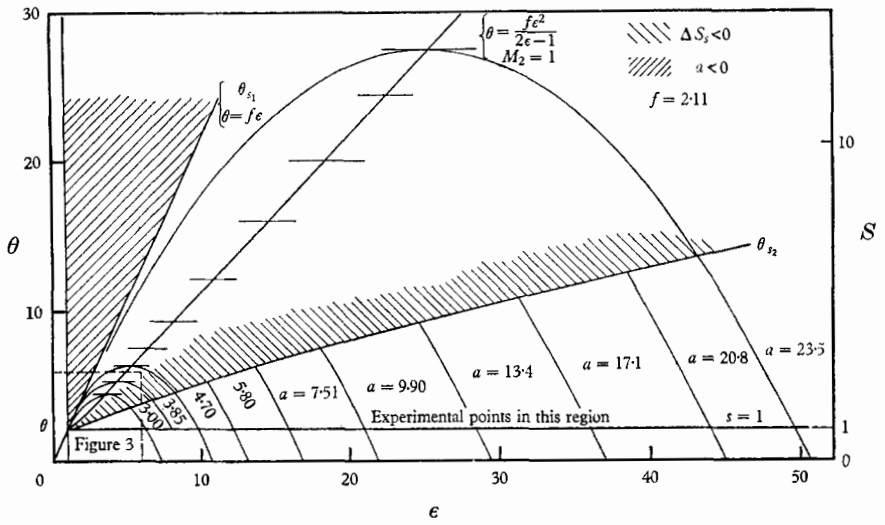

FIGURE 2. Mixing-shock parabolas with possible and impossible regions.

The geometrical locus of these points is found by the elimination of parameter a from the co-ordinates of (2.10). The result is

$$\theta = f\epsilon^2/(2\epsilon - 1). \tag{2.11}$$

The maximum possible compression ratio ϵ_{mx} is reached when $\theta = 0$. The result is

$$\epsilon_{mx} = 1 + af. \tag{2.12}$$

If a mixing-shock parabola is sketched in a (θ, ϵ)-diagram for a certain value of a and f, two solutions of ϵ for each value of θ are found. The physical significance of these solutions may be clarified when the isothermal sound velocity in the mixture after the shock is calculated. The fact that the isothermal instead of the adiabatic sound velocity in such a two-phase mixture must be used was rigorously treated by Plesset & Din (1960, 1961).

For the sound velocity in the mixture after the shock we give the following expression

$$C_{m_2} = (\partial p_2/\partial \rho_{m_2})^{\frac{1}{2}} = u^*\{(\partial \epsilon/\partial \alpha_2)/a\}^{\frac{1}{2}}. \tag{2.13}$$

Using this equation we compute with the aid of (2.6)

$$C_{m_2} = u^*\{(\epsilon+\theta)/(\theta a)^{\frac{1}{2}}\}. \tag{2.14}$$

We remark that $\lim_{\theta \to 0} C''_m = +\infty$. This is caused by the fact that the liquid is assumed to be incompressible, giving an infinitely large sound velocity in the

liquid alone. For finite θ, C''_m is small compared with the actual sound velocities in the liquid and the gas separately. This may be shown by inserting the following current values in (2.14):

$$u^* = 15 \text{ m/sec}, \quad \epsilon = 6, \quad a = 3, \quad \theta = 3, \quad \text{yielding} \quad C_{m_2} = 45 \text{ m/sec}.$$

The mixture velocity after the shock is

$$u_{m_2} = u^*\{(\epsilon+\theta)/\epsilon\}. \tag{2.15}$$

The Mach number in the mixture can now be computed using (2.13) and (2.14). The result is

$$M_2 = u_{m_2} = (a\theta)^{\frac{1}{2}}/\epsilon. \tag{2.16}$$

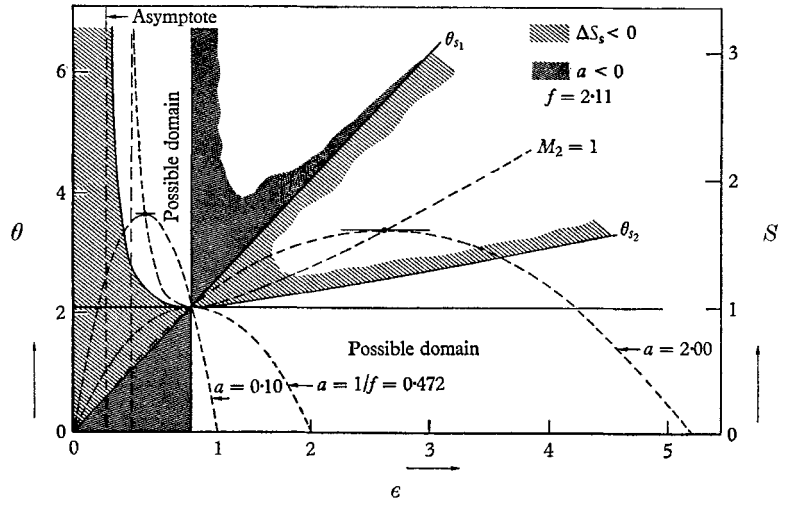

FIGURE 3. Enlarged portion of figure 2 near the origin.

When (2.7) is solved, we obtain

$$\epsilon_{1,2} = \tfrac{1}{2}[(1+af) \pm \{(1+af)^2 - 4a\theta\}^{\frac{1}{2}}]. \tag{2.17}$$

Thus we have two solutions of ϵ for every value of θ and given a and f. Substitution of the θ-ordinate of the tops of the parabolas (2.10) in (2.17) yields

$$\epsilon_{1,2} = (a\theta)^{\frac{1}{2}}\{(\theta_{\text{top}}/\theta)^{\frac{1}{2}} \pm (\langle\theta_{\text{top}}/\theta\rangle - 1)^{\frac{1}{2}}\}, \tag{2.18}$$

which expression combined with (2.16) results in

$$(M_2)_{1,2} = 1/\{(\theta_{\text{top}}/\theta)^{\frac{1}{2}} \pm (\langle\theta_{\text{top}}/\theta\rangle - 1)^{\frac{1}{2}}\}. \tag{2.19}$$

Expressions (2.18) and (2.19) clearly illustrate that on the tops of the parabolas $\epsilon_{1,2} = (a\theta)^{\frac{1}{2}}$, $(M_2)_{1,2} = 1$.

When $\theta < \theta_{\text{top}}$, two possibilities exist: (i) for the + solutions situated on the right-hand branches of the parabolas as shown above, the following holds good: $\epsilon_1 > (a\theta)^{\frac{1}{2}}$, $(M_2)_1 < 1$; (ii) for the − solutions situated on the left-hand branches of the parabolas we have $\epsilon_2 < (a\theta)^{\frac{1}{2}}$, $(M_2)_2 > 1$.

Hence the right-hand branches of the parabolas correspond to subsonic flow after the mixing shock and the left-hand branches to supersonic flow after the shock. It is further observed that (2.11), being the geometrical locus of the tops of the parabolas, is a line of constant Mach number $M_2 = 1$. Observation of the bundle of mixing-shock parabolas in figures 2 and 3 leads to two important problems that will be discussed in the next section. (i) When by a compression mixing shock is meant a shock satisfying $\epsilon > 1$, the question is whether supersonic mixture flow after such a shock is possible. Only subsonic flow is found experimentally. (ii) When by an expansion mixing shock is meant a shock satisfying $0 < \epsilon < 1$, we ask whether such a shock is physically possible.

3. The adiabatic model

In this section, the flow process in the mixing tube will be assumed to be adiabatic. It will be seen that, without heat exchange with the environment, the temperature change as a result of dissipation of kinetic energy in the shock is very small. Beforehand we will assume that the temperature change across the flow process is so small that the relations derived in § 2 which relate mechanical quantities are not changed. Thus only the energy equation (2.4) should be altered. We will now introduce some new symbols:

$\Delta T = T_{l_2} - T_{l_1}$, the temperature change across the mixing shock (degK);
$\gamma = \Delta T_s / T_{l_1}$, dimensionless temperature change;
$\mu = M_g / M_l$, gas–liquid mass flow ratio;
C_l, C_{pg}, specific heat of the liquid and the gas (at constant pressure);
H_l, H_g, total or reservoir enthalpy of liquid or gas;
R_g, the gas constant.

The integral energy balance applied between reference planes $-_1$ and $-_2$ then reads:

$$\left.\begin{aligned} & M_l H_{l_1} + M_g H_{g_1} = M_l H_{l_2} + M_g H_{g_2}, \\ \text{where} \quad & H_{l_1} = p_1/\rho_l + \tfrac{1}{2}u_{l_1}^2 + C_l T_{l_1}, \quad H_{g_1} = \tfrac{1}{2}u_{g_1}^2 + C_{pg} T_{l_1} \\ \text{and} \quad & H_{l_2} = p_2/\rho_l + \tfrac{1}{2}u_{m_2}^2 + C_l(T_{l_1} + \Delta T), \quad H_{g_2} = \tfrac{1}{2}u_{m_2}^2 + C_{pg}(T_{l_1} + \Delta T). \end{aligned}\right\} \tag{3.1}$$

Considering that $\mu \ll 1$ and $\mu C_{pg} \ll C_l$ we may simplify (3.1) to

$$\gamma = \frac{1}{T_{l_1} C_l}\left(\frac{p_1 - p_2}{\rho_l} + \frac{u_{l_1}^2 - u_{m_2}^2}{2}\right). \tag{3.2}$$

Introduction of the quantities ϵ, a, θ, α_2 and ϕ and substitution of (2.6) into (3.2) result in

$$\gamma = \left(\frac{u^{*2}}{2C_l T_{l_1}}\right)\left\{(f^2) - \left(\frac{\theta}{\epsilon}\right)^2\right\}. \tag{3.3}$$

Our expectation that γ is very small is vindicated if we substitute some current values in (3.3). For example with $f = 3, \theta = 3, \epsilon = 5, u^* = 15$ m/sec, $\rho_l = 1000$ kg/m^3, $C_l = 4200$ J/kg, $T_{l_1} = 295$ degK, we compute $\gamma = 0{\cdot}78 \times 10^{-3}$ and $\Delta T_s = 0{\cdot}23$ deg K.

With the aid of expression (3.3) which gives the temperature change explicitly, we may evaluate the entropy change of the flow passing through the shock. Application of the second law of thermodynamics then yields possible and impossible domains in the (ϵ, θ)-diagram. This approach is taken in order to answer the questions raised at the end of § 2.

The entropy change per kg mixture is given by

$$\left.\begin{aligned} &\Delta S = (\Delta S_l + \mu \Delta S_g)/(1+\mu), \\ \text{where} \quad &\Delta S_l = \text{the entropy change of 1 kg liquid} \\ \text{and} \quad &\Delta S_g = \text{the entropy change of 1 kg gas.} \end{aligned}\right\} \tag{3.4}$$

The entropy change of 1 kg liquid is given, after considering that $\gamma \ll 1$, by the expression

$$\Delta S_l = C_l \ln(1+\gamma) \simeq C_l \gamma. \tag{3.5}$$

A similar expression valid for 1 kg gas is

$$\Delta S_g = C_{pg} \ln(1+\gamma) - R_g \ln \epsilon \simeq C_{pg}\gamma - R_g \ln \epsilon. \tag{3.6}$$

Substitution of (3.5) and (3.6) in (3.4) yields, after considering that $\mu C_{pg} \ll C_l$,

$$\Delta S = C_l \gamma - \mu R_g \ln \epsilon. \tag{3.7}$$

From the definition of μ, θ and a we derive the expression

$$\mu = (u^{*2}/R_g T_{l_1})(\theta/a) \tag{3.8}$$

and from (2.7)

$$a = \epsilon(\epsilon - 1)/(f\epsilon - \theta). \tag{3.9}$$

Substitution of (3.9) and (3.8) in (3.7), after some algebraic manipulation, results in the expression of the entropy change per kg mixture passing through the shock

$$\Delta S = (u^{*2}/T_{l_1})\left[\left\{\frac{\ln \epsilon}{\epsilon(\epsilon-1)} - \frac{1}{2\epsilon^2}\right\}\theta^2 - \left(\frac{f \ln \epsilon}{\epsilon - 1}\right)\theta + \tfrac{1}{2}f^2\right] (J/\text{kg deg K}). \tag{3.10}$$

We now want to make use of the second law of thermodynamics, which states that the entropy of an adiabatic process always increases. In symbols this law is given by

$$\Delta S > 0. \tag{3.11}$$

Boundary lines which separate possible from forbidden regions are given by putting $\Delta S = 0$ in (3.10) resulting in an quadratic equation in θ. This equation can be solved, resulting in the two boundary isentropes

$$\theta_{s1} = f\epsilon, \quad \theta_{s2} = \frac{f\epsilon(\epsilon-1)}{2\epsilon \ln \epsilon - \epsilon + 1}. \tag{3.12}$$

In figures 2 and 3 these lines are sketched for $f = 2{\cdot}11$. The following regions may be defined.

For $\epsilon > 1$:

possible $\Delta S > 0$, $0 < \theta < \theta_{s2}$;

impossible $\Delta S < 0$, $\theta_{s2} < \theta < \theta_{s1}$.

For $0 < \epsilon < 1$:

possible $\Delta S > 0$, $\theta > \theta_{s2}$;

impossible $\Delta S < 0$, $\theta_{s1} < \theta < \theta_{s2}$.

Additional impossible regions are found where the Euler number a is negative. These regions are, for $\epsilon > 1$, $\theta > \theta_{s1}$ and, for $0 < \epsilon < 1$, $0 < \theta < \theta_{s1}$. The net result of this is that only two possible domains are left: for $\epsilon < 1$, $0 < \theta < \theta_{s2}$ and, for $0 < \epsilon < 1$, $\theta > \theta_{s2}$.

The question of whether supersonic flow after a compression mixing shock is possible can now be answered. It can be easily seen that, for all values of $\epsilon > 1$, the θ_{s2} isentrope is situated below the line of constant Mach number $M_2 = 1$ given by (2.11), or, when

$$\epsilon > 1, \quad \frac{f\epsilon(\epsilon-1)}{2\epsilon\ln\epsilon-\epsilon+1} < \frac{f\epsilon^2}{2\epsilon-1}. \tag{3.13}$$

This implies that the θ_{s2} isentrope crosses only the right-hand branches of the parabolas yielding subsonic solutions. Hence in the domain $\epsilon > 1$, $0 < \theta < \theta_{s2}$ no supersonic solutions can be found.

This leaves us with the possible domain for an expansion mixing shock $0 < \epsilon < 1$, $\theta > \theta_{s2}$. However, when $0 < \epsilon < 1$, we have, according to (2.5), $\alpha_2 < \phi$ which results in $u_{l_1} < u_{m_2}$. It will be seen that this is contradictory to the gas entrainment mechanism proposed in § 5.

4. Shock stability

An important question is what parameters influence the stability of the shock which is located at a position defined by the length co-ordinate x. It was felt that, in order to answer this question, wall friction must be introduced into our considerations. In order to perform the stability calculation we will introduce the pressure gradient in the jet flow $(\partial p/\partial x)_1$ and in the froth flow $(\partial p/\partial x)_2$. Let the shock be submitted to small pressure oscillations Δp upstream with phase angle ωt, t denoting time and ω circular frequency. These pressure oscillations will result in small deviations of the shock front position $\Delta y = y$ and in a small shock front speed $\Delta u = dy/dt$; see figure 4. The oscillations of the shock front take place between two fixed control planes A and B.

In the calculations we will take into account the changing fluid mass ΔM_s inside the two reference planes. Thus we write down for the continuity equation

$$M_{l_2} = M_{l_1} + \Delta M_s. \tag{4.1}$$

Using (4.1) the momentum equation yields

$$(p_1 A_{mt} + M_{l_1} u_{l_1}) - \{p_2 A_{mt} + (M_l + \Delta M_s)(u_{l_2} + \Delta u)\} = \int_0^t \Delta M_s \frac{\partial}{\partial t} \Delta u \, dt, \tag{4.2}$$

which results in

$$(p_1 A_{mt} + M_{l_1} u_{l_1}) - (p_2 A_{mt} + M_{l_1} u_{l_2}) - 2M_{l_1}\Delta u - 2\Delta M_s \Delta u = \int_0^t \Delta M_s \frac{\partial}{\partial t} \Delta u \, dt. \tag{4.3}$$

Neglecting second-order terms and introducing the symbols ϵ, a, ϕ, u^* and θ, we arrive at the situation at time t

$$\epsilon^2 - \epsilon\left\{1 + a\left(f - \frac{2\Delta u}{u^*}\right)\right\} + a\theta = 0. \tag{4.4}$$

Defining $\quad \bar{\epsilon} = \bar{p}_2/\bar{p}_1, \quad \bar{a} = \rho_l u^{*2}/\bar{p}_1, \quad \bar{\theta} = \bar{Q}_{g_1}/Q_{l_1},$

$$p_2 = \bar{p}_2 - (\partial p/\partial x)_2 \Delta y, \quad p_1 = \bar{p}_1 + \Delta p \sin\omega t + (\partial p/\partial x)_1 \Delta y,$$

we derive the following expressions for ϵ, a and θ in (4.4):

$$\left.\begin{aligned} \epsilon &= \frac{\bar{\epsilon}-\xi_2\Delta y}{1+\Delta\alpha\sin\omega t+\xi_1\Delta y}, \quad a = \frac{\bar{a}}{1+\Delta\alpha\sin\omega t+\xi_1\Delta y}, \quad \theta = \frac{\bar{\theta}}{1+\Delta\alpha\sin\omega t+\xi_1\Delta y}, \\ \text{where} \quad & \Delta\alpha = \Delta p/\bar{p}, \quad \xi_1 = (1/\bar{p}_1)(\partial p/\partial x)_1, \quad \xi_2 = (1/\bar{p}_1)(\partial p/\partial x)_2. \end{aligned}\right\} \tag{4.5}$$

Substitution of (4.5) in (4.4), after multiplication of both sides by

$$(1+\Delta\alpha\sin\omega t+\xi_1\Delta y)^2,$$

results in

$$(\bar{\epsilon}-\xi_2\Delta y)^2-(\bar{\epsilon}-\xi_2\Delta y)\{1+\Delta\alpha\sin\omega t+\xi_1\Delta y+\bar{a}[f-(2\Delta u/u^*)]\}+\bar{a}\bar{\theta}=0; \tag{4.6}$$

when $t=0$ we have

$$\bar{\epsilon}^2-\bar{\epsilon}(1+\bar{a}f)+\bar{a}\bar{\theta}=0. \tag{4.7}$$

Subtracting (4.6) from the initial condition (4.7) gives the relation between the first-order terms.

After denoting $\Delta y = y$, $\Delta u = dy/dt$, $\bar{M}_2 = (\bar{a}\bar{\theta})^{\frac{1}{2}}/\bar{\epsilon}$, where $\bar{M}_2$ is the Mach number in the average flow after the shock, we arrive at the following differential equation:

$$(dy/dt)-vy = w\sin\omega t \tag{4.8}$$

with the solution

$$\left.\begin{aligned} y &= \left(\frac{w}{v^2+\omega^2}\right)\{\omega\, e^{vt}-v\sin\omega t-\omega\cos\omega t\}, \\ \text{where} \quad & w = (u^*/2\bar{a})\,\Delta\alpha \text{ and } v = (u^*/2\bar{a})\{\xi_1-2\xi_2(1-\bar{M}_2)\}. \end{aligned}\right\} \tag{4.9}$$

From this result it is clear that when ξ_1 and $\xi_2 \neq 0$ and $t \to +\infty$:

$$\begin{aligned} v<0, \quad & \bar{M}_2 < 1+(\xi_1/2\xi_2), \quad \text{stable position;} \\ v>0, \quad & \bar{M}_2 > 1+(\xi_1/2\xi_2), \quad \text{unstable position.} \end{aligned}$$

In practical cases $\xi_1/2\xi_2 \ll 1$ since the jet flow barely touches the channel wall and the stable position is associated with subsonic flow after the shock, the unstable position with supersonic flow after the shock.

5. The gas entrainment mechanism in the mixing shock

From the previous sections we know that the experimental points should lie on the mixing shock parabolas outside the forbidden regions. Up until now we cannot predict the location of the experimental points on these parabolas. We will start with the following model.

It is postulated that the shock can only exist when the jet flow impinges on a free surface which prevents the jet flow from penetrating further. It is further assumed that the gas entrainment mechanism is similar to air enclosure during the impact of a water droplet on a free surface. On this subject extensive work was done recently by Engel (1966, 1967). Figure 5(*a*) which was taken from Engel's work gives a schematic view of the flow process involved. From the experimental data presented in these papers we have concluded the following: (i) cavity closure occurs when cavity depth is nearly maximal; (ii) in that position the kinetic energy of the fluid surrounding the cavity is very small and may be

neglected; (iii) the viscous energy which is dissipated between the time of droplet impact and the time of cavity closure is small enough to be neglected.

To these statements we add the following assumptions:

The process is isothermal. This means that extra free energy is needed to generate the surface area in comparison with an isentropic process. The thickness

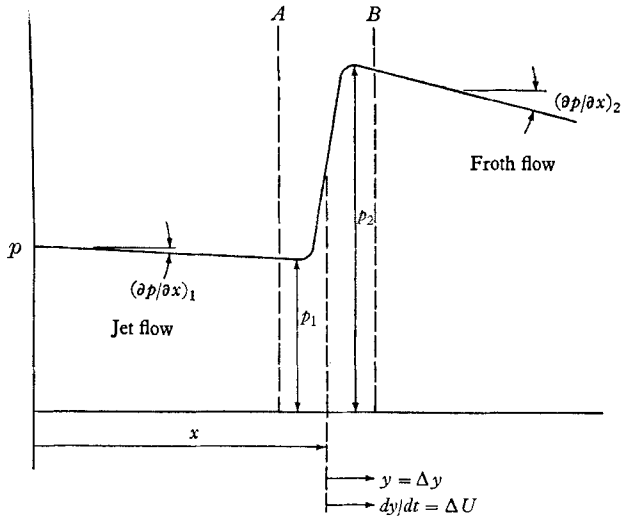

FIGURE 4. Mixing shock oscillating between two control planes A and B.

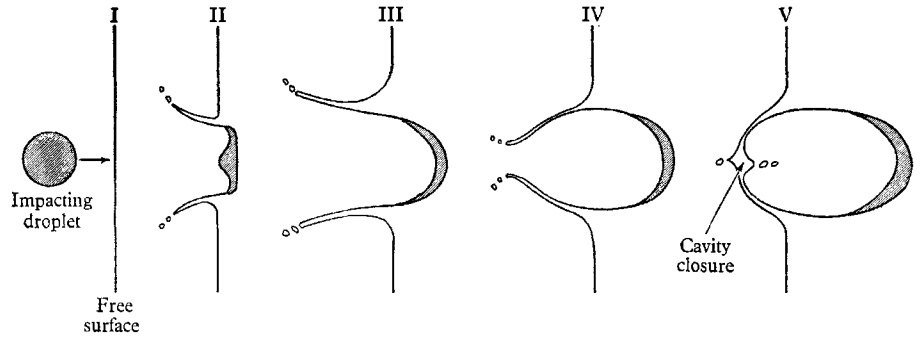

FIGURE 5(*a*). Proposed gas entrainment mechanism taken from Engel (1966, 1967).

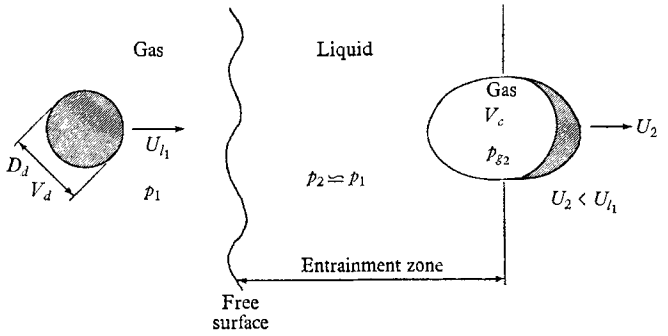

FIGURE 5(*b*). Conditions before and after the entrainment zone.

of the entrainment zone is small compared with the thickness of the shock as a whole. This means that we may equate the gas pressure to the liquid pressure immediately behind the free surface or $p_1 \simeq p_2$.

Another sweeping assumption is that spherical bubbles will leave the entrainment zone without slip with the surrounding liquid phase.

The role of gravity will be neglected since $gD_{mt}/u_{l_1}^2 \ll 1$. In our experiments the mixing tube diameter D_{mt} amounted to 0·03 m; u_{l_1} was in the range of 30–70 m/sec; see also figure 5(*b*).

Using these assumptions the energy balance of a spherical droplet taken before impact and after leaving the entrainment zone, reads

$$E_{k_1} - E_\sigma - E_c - E_{k_2} = 0, \tag{5.1}$$

where E_{k_1} and E_{k_2} are the kinetic energies of the in- and out-going droplet, E_c is the energy needed to compress the gas by surface tension and E_σ is the extra surface energy which must be supplied for increasing the liquid–gas interface.

Denoting the cavity volume by V_c and the droplet volume by V_d, we may write down the four contributions to the energy equation:

$$E_{k_1} = \tfrac{1}{2}\rho V_d (u^*/\phi)^2, \tag{5.2}$$

$$E_{k_2} = \tfrac{1}{2}\rho V_d u^{*2}\{1 + (V_c/V_d)\}^2, \tag{5.3}$$

$$E_\sigma = \pi(6/\pi)^{\frac{2}{3}}\{\sigma - T_{l_1}(\partial\sigma/\partial T_{l_1})\}(V_c^{\frac{2}{3}} - V_d^{\frac{2}{3}})\}, \tag{5.4}$$

$$E_c = p_1 V_c \ln\left[1 + \{4\sigma/\langle(\rho u^{*2}/a)(6/\pi)^{\frac{1}{3}} V_c^{\frac{1}{3}}\rangle\}\right]. \tag{5.5}$$

In these expressions the isentropic surface tension $\sigma = 0{\cdot}072$ N/m, $T_{l_1} = 293$ degK and $\partial\sigma/\partial T_{l_1} = -0{\cdot}0001425$ N/m degK. Substitution of (5.2) to (5.5) in (5.1) yields an equation in V_c which may be solved numerically for given V_d, u^*, a, ϕ, σ. Once V_c is found the volume flow ratio θ and velocity ratio S before the shock can be computed using the following expressions:

$$\theta = (V_c/V_d)\left[1 + \{4\sigma/\langle(\rho u^{*2}/a)(6/\pi)^{\frac{1}{3}} V_c^{\frac{1}{3}}\rangle\}\right], \tag{5.6}$$

$$S = \theta \Big/ \left(\frac{1}{\phi} - 1\right). \tag{5.7}$$

Figure 6 gives the results of the numerical calculations, and shows the slip factor S as a function of the Euler number a for four droplet diameters 10, 1, 0·3, 0·1 mm and four values of ϕ, 0·360, 0·322, 0·284, 0·250. We also computed the Mach number immediately after the entrainment zone. From these data we see that the results are nearly independent of the numerical value of ϕ. The theory predicts a slip factor slightly larger than 1 and slowly increasing with increasing Euler number a. It will be shown in the next section that this trend is supported by experimental evidence. An important result is that we predict supersonic flow after the entrainment zone. It is stressed that the last result is not in contradiction with the entropy considerations of § 3, which only forbid supersonic flow when the mixture leaves the mixing shock. Finally, it is seen that the concept of an expansion mixing shock is not compatible with the mechanism described here. First, for an expansion mixing shock we have $u_{m_2} > u_{l_1}$. Denoting the mixture velocity after the entrainment zone by u_2, according to the present model

$u_2 > u_{m_2}$; we thus obtain the requirement $u_{l_1} < u_2$. We do not see how this inequality can be realized since surface tension energy is withdrawn from the kinetic energy of the incoming droplet stream.

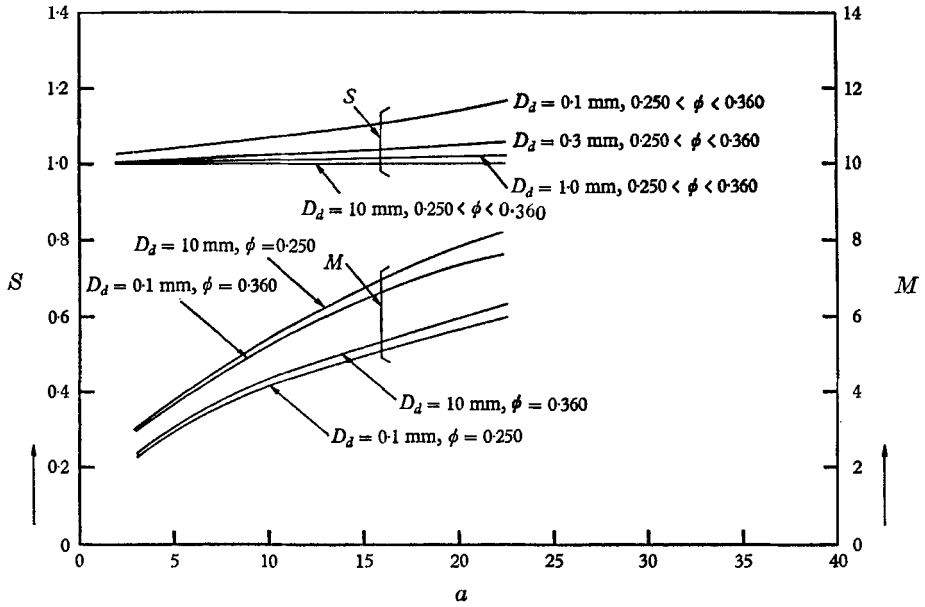

FIGURE 6. Slip factor and Mach number after the entrainment zone.

6. The cavitation shock

By simply closing the gas valve of the ejector we can generate a particular type of mixing shock. Before this shock we have jet flow in which only vapour is present. As in the case of the mixing shock bubbles are created but these implode spontaneously and the vapour contained in the bubbles condenses. This is caused by the fact that the pressure behind the shock is higher than the saturated vapour pressure in the liquid. Thus after the shock only liquid is left. For obvious reasons we have called the phenomenon cavitation shock. The compression ratio across such a shock simply follows from (2.5) with $\alpha_2 = 0$, and $p_1 = p_v$ where p_v denotes the saturated vapour pressure. The result is

$$\epsilon = 1 + af, \quad \text{where} \quad \epsilon = p_2/p_v, \quad a = \rho u^{*2}/p_v. \tag{6.1}$$

Since $M_2 = 0$ after the shock for an incompressible liquid, the shock is stable according to (4.9) if $\xi_1/2\xi_2 < 1$. ϵ may be very high in this case; for example, with $u^* = 15{\cdot}6$ m/sec, $\rho_l = 1000\,\text{kg/m}^3$, $p_v = 2300\,\text{N/m}^2$, $f = 2{\cdot}11$, we find $\epsilon = 215$. Some experimental data that confirm (6.1) will be given in the next section.

7. Experimental results

A detailed description of the flow circuit and measuring errors can be found in the author's thesis (Witte 1962). A schematic view of the test assembly is given in figure 1. The air enters the suction chamber after passing a quarter-circle

orifice plate and a throttle valve. The water is injected by a high pressure (30 atm) pump; it passes a globe valve, which is used to adjust the pump discharge, and flows through an orifice plate to the nozzle situated in the suction chamber of the ejector. The air mass flow rate is measured with the aid of two quarter-circle orifice plates, together with a barometer and a thermometer. The pressure along the flow channel is measured with 12 Bourdon manometers with a range of 0–10 atm. The suction chamber pressure can be determined with a U tube filled with mercury and a barometer; one end of the U tube is in open connexion with the atmosphere and the other end is connected to the suction chamber. The water temperature is measured with a calibrated thermometer with a range of 0–50 °C.

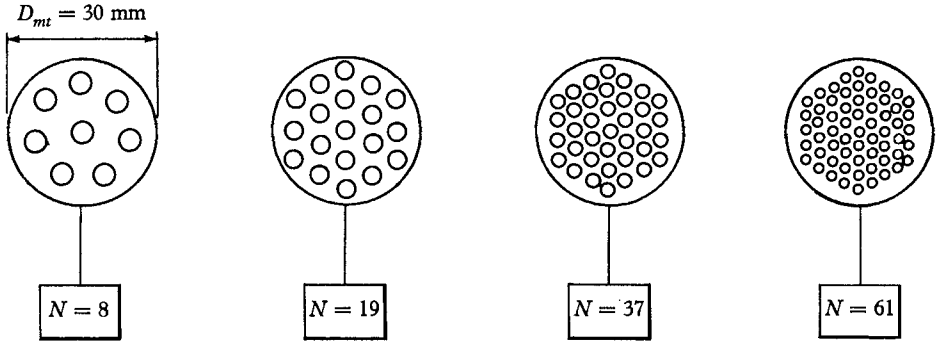

FIGURE 9. Location of nozzle exit areas relative to channel wall.

In order to photograph the flow phenomena a Perspex mixing tube was used. A stroboscopic light source was used for producing flashes with a duration of 3×10^{-6} sec measured at $\frac{1}{3}$ of the peak intensity. The results are shown in figures 7 and 8, plate 1. The experiments were carried out in such a manner that parameter a is adjusted and ϵ and θ measured. The back pressure is adjusted so as to make the end of the mixing zone coincide with the end of the mixing tube. This may be checked by reading the manometers along the mixing tube. The corresponding adjustment was maintained in all test runs.

During the experiments we changed the numbers of holes N in one nozzle; figure 9 gives the shape of the different nozzle exit areas. Nozzles with 8, 19, 37 and 61 holes were tested. The experiments were done for three different Reynolds numbers, $\rho u_{l_1} D_n/\eta_l$, where D_n denotes the superficial nozzle diameter and η_l the liquid viscosity. The nozzle area ratio ϕ and the Euler number a were also varied.

Two programs were run:

$D_{mt} = 0{\cdot}03$ m (mixing-tube diameter), $\phi = 0{\cdot}322$, $N = 8, 19, 37, 61$, $Re = 7, 8, 9 \times 10^5$, $a = 3{\cdot}0, 3{\cdot}85, 4{\cdot}70, 5{\cdot}80, 7{\cdot}51, 9{\cdot}90, 13{\cdot}4, 17{\cdot}1, 20{\cdot}8, 23{\cdot}5$. This program results in 120 points in an (ϵ, θ)-diagram.

The other program was:

$D_{mt} = 0{\cdot}30$ m, $\phi = 0{\cdot}250, 0{\cdot}284, 0{\cdot}322, 0{\cdot}360$, $N = 8, 19, 37, 61$, $Re = 9 \times 10^5$, $a = 3{\cdot}0, 3{\cdot}85, 4{\cdot}70, 5{\cdot}80, 7{\cdot}51, 9{\cdot}90, 13{\cdot}4, 17{\cdot}1, 20{\cdot}8, 23{\cdot}5$, yielding 160 points in an (ϵ, θ)-plot.

The results of the first program are shown in figure 10. This diagram gives a view of the experimental points relative to the corresponding right-hand branches

of the mixing-shock parabolas. It is remembered that these branches yield subsonic solutions. It is seen that these experimental points are all located within 5 % of these lines. This gives an experimental proof of (2.7) and illustrates that the flow behind a compression mixing shock is subsonic.

It is seen that changes in Re and N do not influence the results to a large extent. We observe that S and θ increase slowly with increasing a and ϵ. From the results

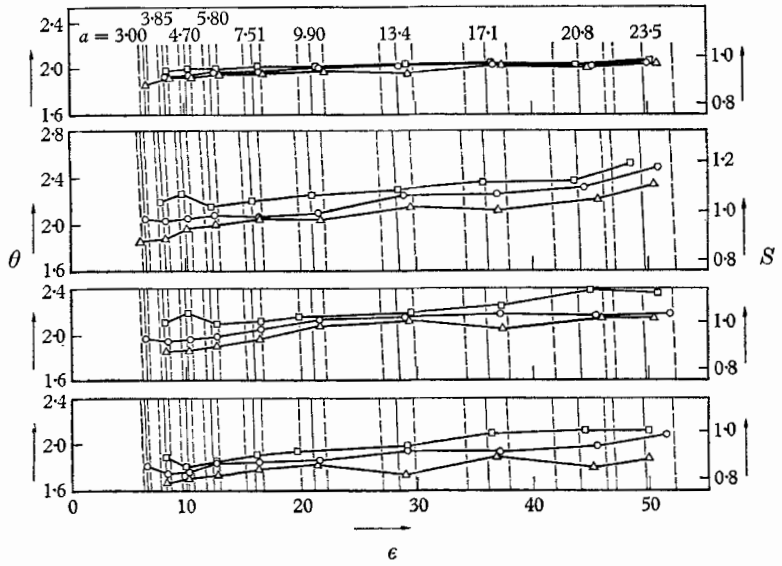

FIGURE 10. Results of the first test program. □, $Re = 9{\cdot}00 \times 10^5$; ○, $Re = 8{\cdot}00 \times 10^5$; △, $Re = 7{\cdot}00 \times 10^5$; – – – –, 5 % error line.

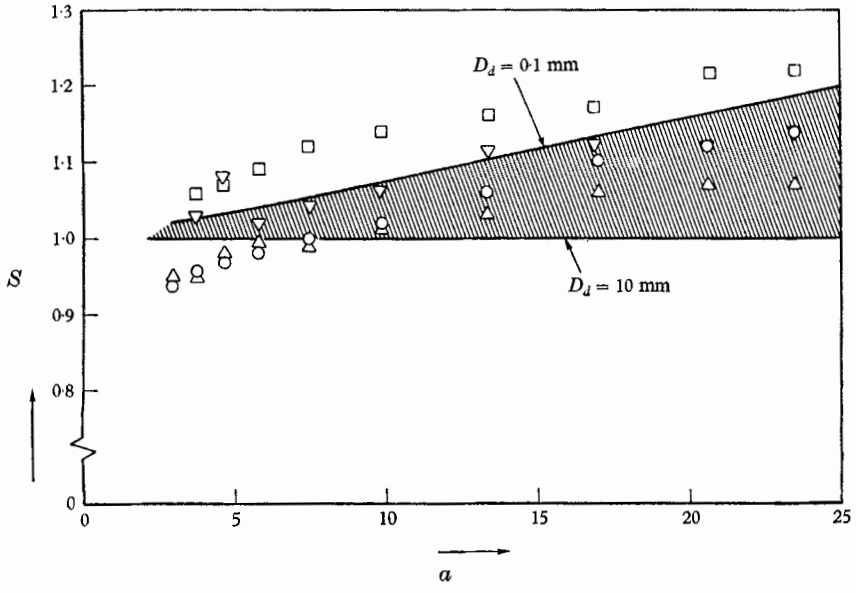

FIGURE 11. Comparison of the measured data with the theoretical predictions given in figure 6. ○, $\phi = 0{\cdot}250$; △, $\phi = 0{\cdot}284$; ▽, $\phi = 0{\cdot}322$; □, $\phi = 0{\cdot}360$.

of the second program similar conclusions can be drawn, in addition to the fact that changing ϕ does not influence S to a great extent. Since this behaviour is also evident from figure 10, another (θ, ϵ)-plot similar to figure 10 is omitted.

For comparing the amount of air which is swallowed by the shock with the predicted values, we have gathered the results of the following experiments in one diagram:

$D_{mt} = 0{\cdot}03, \quad Re = 9 \times 10^5, \quad N = 19;$

$\phi = 0{\cdot}250, \quad 0{\cdot}284, \quad 0{\cdot}322, \quad 0{\cdot}360;$

$a = 3{\cdot}0, \quad 3{\cdot}85, \quad 4{\cdot}70, \quad 5{\cdot}80, \quad 7{\cdot}51, \quad 9{\cdot}90, \quad 13{\cdot}4, \quad 17{\cdot}1, \quad 28{\cdot}0, \quad 23{\cdot}5.$

These data are compared with the theoretical prediction of the gas entrainment rate as a function of the Euler number a for different droplet sizes, given in figure 6 for the same parameters.

In figure 11 it is seen that for a wide range of droplet sizes, 0·1–10 mm, the results compare reasonably well. For comparison, the diameters of the individual nozzle holes were of the order of 3–4 mm during these experiments.

The results of the experiments with the cavitation shock can best be illustrated in the following table.

$D_{mt} = 0{\cdot}03$ m, $\phi = 0{\cdot}322$, $p_v = 2650$ N/m²

N	M_{l_1}(kg/sec)	ϵ measured	ϵ calculated
8	11·1	192	196
19	11·1	196	196
37	11·1	192	196
61	11·1	192	196

Here, the deviation between the measured and the calculated values of the pressure ratio is not more than 2 %.

8. Concluding remarks

Since from current experimental data supersonic flow is predicted after the entrainment zone, a compression shock must be present in order to obtain the predicted subsonic mixture flow. The two-phase compression shock was described by Campbell & Pitscher (1958).

Figures 7 and 8 give photographs of the mixing shock and the cavitation shock taken through a transparent cylindrical mixing tube. Figure 7 shows the free surface which stands perpendicular to the flow direction at the wall of the mixing tube. Figure 8 shows the region of imploding bubbles in the cavitation shock.

A detailed study of the structure of the mixing shock using an ultra-high-speed camera combined with a two-dimensional transparent flow channel was carried out by Rynders (1965). From his photographs, the free surface and the imploding bubbles and bubble clouds can be clearly seen. An interesting result of this investigation is that the free surface is only perpendicular to the flow direction at the channel walls. Proceeding inward the free surface curves backward in the

direction of the flow, forming a trough-like shape with its apex at the centre of the channel.

From the photographs we could not get any proof of the existence of the entrainment zone. Probably these free surface processes were going too fast to be filmed. Thus only the indirect evidence of §§ 5 and 7 can be presented.

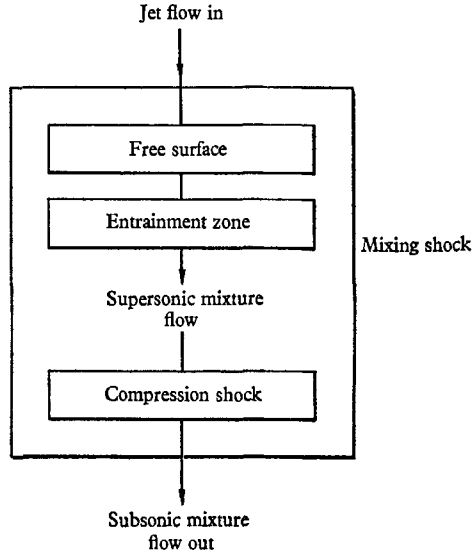

FIGURE 12. Schematic view of the mixing shock.

Figure 12 gives a schematic view of the processes in the mixing shock as proposed in this paper.

This paper is partly based on the author's thesis presented at Delft Technological University. He is greatly indebted to Prof. J. O. Hinze for his help and advice in this investigation.

REFERENCES

CAMPBELL, I. J. & PITSCHER, A. S. 1958 Shock waves in a liquid containing gas bubbles. *Proc. Roy. Soc.* A **243**, 534.

ENGEL, O. G. 1966 Crater depths in fluid impacts. *Appl. Phys.* **37**, no. 4.

ENGEL, O. G. 1967 Initial pressure, initial flow velocity and the time dependence of crater depth in fluid impacts. *J. Appl. Phys.* **38**, no. 10.

PLESSET, M. S. & DIN, Y. H. 1960 Theory of gas bubble dynamics in oscillating pressure fields. *Phys. Fluids*, **6**, 882.

PLESSET, M. S. & DIN, Y. H. 1961 On the propagation of sound in a liquid containing gas bubbles. *Phys. Fluids*, **8**, 970.

RYNDERS, J. P. 1965 Research on the physical processes in the two phase mixing shock. Ingenieur Thesis, Delft Technological University.

VON PAWELL, R. G. 1936 Dissertation, Brunswick.

WITTE, J. H. 1962 Mixing shocks and their influence on the design of liquid gas ejectors. Dissertation, Delft.

WITTE, J. H. 1965 Efficiency and design of liquid gas ejectors. *Br. Chem. Engng.* **10**, no. 9.

WITTE, J. H. 1966 Shock phenomena in two phase flows. *Royal Institute of Engineers Symposium, Two Phase Flows, Delft.*

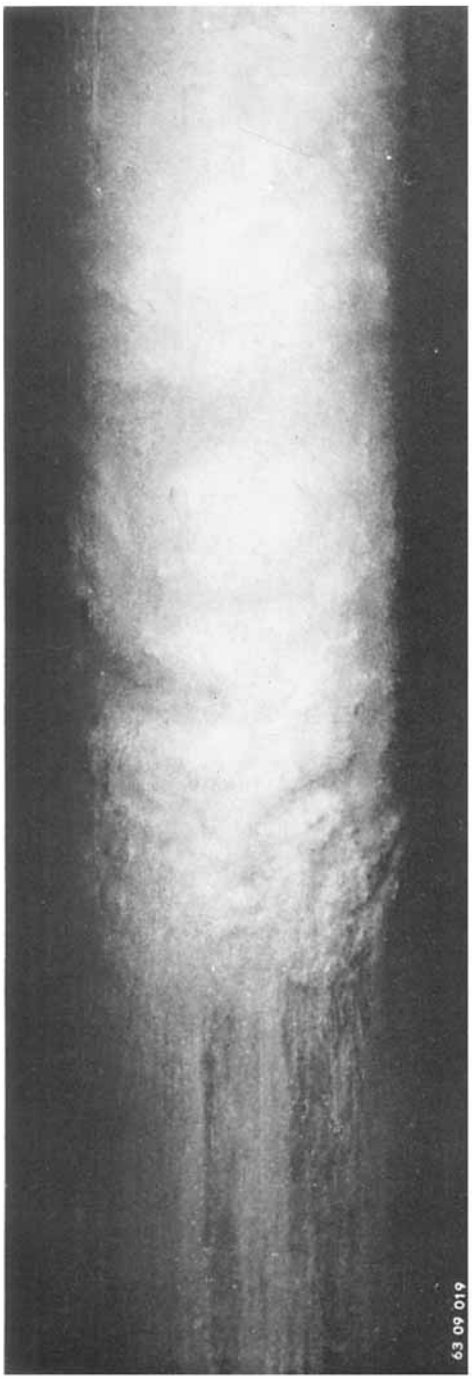

FIGURE 7. Mixing shock. $a = 23{\cdot}5$, $\epsilon = 78{\cdot}0$, $\theta = 3{\cdot}44$, $\phi = 0{\cdot}250$, $M_l = 11{\cdot}1$ kg/sec, $D_n = 15$ mm. Flow from left to right. Exposure time 3×10^{-6} sec. Black velvet background.

FIGURE 8. Cavitation shock. $a = 118$, $\epsilon = 270$, $\phi = 0{\cdot}322$, $M_l = 12{\cdot}5$ kg/sec. Black velvet background.

(*Facing p.* 656)